Nontrivial scaling in supply limited Aeolian sand transport

Sandesh Kamath[1], Yaping Shao[1], Eric J. R. Parteli[2]

[1]Institute of Geophysics and Meteorology, University of Cologne, Germany
[2]Faculty of Physics, University of Duisburg-Essen, Germany

Key Points:

- We introduce a particle-based model in investigating Aeolian (wind-blown) sand transport when the sand cover on the soil is sparse
- The scaling of the Aeolian transport rate with the wind shear velocity has a non-trivial exponent depending on the sand cover thickness
- There is an anomaly in the functional dependence of the transport rate on the sand cover thickness, depending on the rigid ground roughness

Corresponding author: Sandesh Kamath, `skamath@uni-koeln.de`

Abstract

Previous studies of wind-blown sand have considered either fully erodible or non-erodible soils, but the transport over sparsely sand-covered soils is still poorly understood. The quantitative modeling of this transport is important for the parametrization of Aeolian processes under limited sediment supply in climate models. Here we show, by means of particle-based numerical simulations, that the Aeolian sand transport rate scales with the wind shear velocity u_* as $(u_* - u_{*\mathrm{t}})^p \cdot \left[u_*^2 - u_{*\mathrm{t}}^2\right]$, where $u_{*\mathrm{t}}$ is the minimal threshold u_* for sustained transport, and the exponent p is a non-linear function of the mobile sand cover thickness. Specifically, we find that the scaling of the Aeolian sand transport rate with u_* increases from quadratic to cubic as soil conditions change from fully erodible to rigid. Furthermore, this scaling is affected by the roughness of the non-erodible ground, thus providing constraints for modeling supply limited soils.

Plain Language Summary

The transport of sand by wind shapes the Earth's surface and constitutes one major factor for the emission of dust aerosols. The accurate modeling of wind-blown sand transport is thus important to achieve reliable climate simulations and to make predictions about the propagation of desertification. Previous models of wind-blown sand were designed to compute sand transport rates over a thick sand layer, such as the surface of large, active sand dunes. However, natural soils encompass a broad range of limited sand supply conditions, such as crusted or bare soils. It has been a long-standing open question how wind-blown sand transport rates respond to wind velocity when the bare ground is covered by a thin layer of sand. Here we calculate the trajectories of wind-blown sand grains and find that sand transport rates increase faster with wind speed under supply limited conditions than over sand dunes. The reason for this behavior is elucidated in our simulations: The hopping sand grains fly higher the less sand is covering the hard surface. We obtain mathematical expressions for the sand transport rates as a function of the thickness of sand covering the bare soil, which will be important to improve climate models.

1 Introduction

Aeolian (wind-blown) sand transport produces ripples and dunes and plays a vital role in shaping the Earth's surface. This transport occurs mainly through sand grains hopping along the surface (saltation), thereby transferring to the ground momentum that may set new particles into hopping, rolling or sliding motion (Bagnold, 1941; Shao, 2008; Kok et al., 2012). Furthermore, the particle splash generated by saltating grains provides one main mechanism of dust aerosol emission (Gillette, 1981; Shao et al., 1993), which has major feedbacks with the biosphere, the hydrological cycle and various other components of the Earth system (Mahowald et al., 2014; Schepanski, 2018). The accurate modeling of wind-blown sand is, thus, important for the development of reliable geomorphodynamic, climate and Earth system models (Shao, 2008).

Indeed, previous models of Aeolian sediment transport focused mainly on the transport over either fully erodible beds, such as migrating dunes and ripples (Anderson & Haff, 1988; Shao & Li, 1999; Sauermann et al., 2001; Almeida et al., 2008; Kok & Renno, 2009; Lämmel et al., 2012; Pähtz et al., 2014; Comola et al., 2019), or rigid, fully non-erodible beds, such as consolidated dunes and bare soils (Ho et al., 2011). These studies have shown that wind-blown transport rates follow either a quadratic or a cubic scaling with the wind shear velocity — which is proportional to the mean flow velocity gradient in turbulent boundary layer flow — depending upon the bed being fully erodible or fully non-erodible, respectively (Creyssels et al., 2009; Ho et al., 2011). However, natural Aeolian systems encompass a broad range of soil types subjected to limited sediment supply conditions, including crusted or bare soils sparsely covered with mobile sand (Shao, 2008; Amir et al., 2014). The characteristics of

Aeolian sand transport over such types of soil, i.e., when the thickness of the mobile sand layer on the rigid ground is comparable to a few grain diameters, are poorly understood.

Therefore, here we perform the direct computation of grain trajectories during Aeolian sand transport by means of particle-based simulations, or Discrete-Element-Method (DEM). This type of simulation has been applied previously to investigate Aeolian transport over fully erodible beds (Carneiro et al., 2011; Durán et al., 2012; Comola et al., 2019). However, here we present a DEM simulation for Aeolian sand transport under low availability of mobile sand. We show here that the thickness of the mobile sand layer, $h_{\rm mob}$, has considerable and yet unreported impact on the scaling law of the sand transport rate with the wind shear velocity. As we will show in the subsequent sections, this scaling is characterized by a nontrivial exponent dependent on $h_{\rm mob}$, with implications for climate models and wind tunnel experiments.

2 Numerical experiments

The Discrete-Element-Method consists of solving the Newton's equations of motion for all particles in the system under consideration of the main forces acting on them (Cundall & Strack, 1979). In contrast to other types of numerical models of soil erosion (Anderson & Haff, 1988; Almeida et al., 2008; Kok & Renno, 2009), DEM models of Aeolian sand transport do not rely, thus, on a splash function to represent the ejection of particles from the soil owing to grain-bed collisions. Rather, the lift-off velocities of the rebound and ejected particles are obtained by directly solving their equations of motion under consideration of particle-particle interactions (Lämmel et al., 2017; Yin et al., 2021).

In this section we explain the main features of our simulations, while the details about the DEM method and the integration of the equations of motion are reviewed in the Supplemental Material. We start our simulations by pouring sand-sized spherical particles of diameter d uniformly distributed in the range $160 \leq d/\mu\mathrm{m} \leq 240$ onto a flat horizontal rigid bed at the bottom of the simulation domain — which has dimensions $(L_x \times L_y \times L_z)/d_{\rm m} = (200 \times 8 \times 1000)$, with $d_{\rm m} = 200\,\mu$m denoting the mean grain size (Fig. 1). In doing so, we generate a thin bed of $N_{\rm p}$ randomly poured particles on the ground, where the bed thickness $h_{\rm mob}$ is determined by $N_{\rm p}$. For instance, $N_{\rm p} = 30,000$ for the largest bed thickness investigated here, i.e., $h_{\rm mob} \approx 15\,d_{\rm m}$.

Furthermore, we adopt periodic boundary conditions in the along-wind (x) and cross-wind (y) directions and impose a reflective horizontal wall at the top of the simulation domain, to avoid that particles escape through crossing the upper boundary at $z = L_z$. However, we find that removing this reflective wall would allow only few particles for escaping, thus leading to a negligible change in the results of our simulations.

Once the particles come to rest and the bed has been formed, a few particles are injected into the simulation domain to impact on the ground; thus producing a splash and ejecting grains into air. The Aeolian drag force on the particles is computed with the expression,

$$\mathbf{F}_i^{\rm d} = -\frac{\pi d^2}{8}\rho_{\rm f} C_{\rm d} \upsilon_{\rm r} \mathbf{v}_{\rm r}, \tag{1}$$

where $\rho_{\rm f} = 1.225\,\mathrm{kg/m^3}$ is the air density, $\mathbf{v}_{\rm r} = \mathbf{v}_{\rm p} - \mathbf{u}$, with $\mathbf{v}_{\rm p}$ and $\mathbf{u}$ denoting the velocities of the particle and the fluid, respectively. Furthermore, $\upsilon_{\rm r} = |\mathbf{v}_{\rm r}|$, and $C_{\rm d}$ is the drag coefficient, which is computed using the following model (Cheng, 2009),

$$C_{\rm d} = \left[\left(\frac{32}{\rm Re}\right)^{2/3} + 1\right]^{3/2}, \tag{2}$$

where the Reynolds number $\mathrm{Re} = \rho_{\rm f}\upsilon_{\rm r} d_{\rm m}/\mu$, with $\mu = 1.8702 \times 10^{-5}\,\mathrm{kg\,m^{-1}s^{-1}}$ denoting the dynamic viscosity of the air. The wind velocity profile is constant along x and y throughout the simulations, while the initial vertical profile of the horizontal (downstream) wind velocity, $u_x(z)$, is logarithmic, i.e.,

$$u_x(z) = \frac{u_*}{\kappa} \ln \frac{z - h_0 + z_0}{z_0} \tag{3}$$

where u_* is the wind shear velocity, $\kappa = 0.4$ the von Kármán constant, $z_0 \approx d_\mathrm{m}/30$ is the roughness of the quiescent bed, and h_0 is the bed height, which is set as the uppermost height within the granular surface where the particles move with velocity smaller than $0.1\,u_*$ (Carneiro et al., 2011). However, the acceleration of the particles owing to the action of the drag force extracts momentum from the air (Owen, 1964; Anderson & Haff, 1988), thus leading to a modification of the wind velocity profile. The modified velocity profile is obtained by numerical integration of (Carneiro et al., 2011)

$$\frac{\partial u_x}{\partial z} = \frac{u_{\tau,x}(z)}{\kappa z};\; u_{\tau,x}(z) = u_* \left[1 - \frac{\tau_\mathrm{p}(z)}{\rho_\mathrm{f} u_*^2}\right]^{1/2}, \tag{4}$$

where $\tau_\mathrm{p}(z)$ is the grain-borne shear stress and is given by

$$\tau_\mathrm{p}(z) \approx \sum_{i:z_j>z} \frac{F_{i,x}^\mathrm{d}}{A}, \tag{5}$$

with $F_{i,x}^\mathrm{d}$ denoting the horizontal component of the drag force on particle i and $A = L_x \cdot L_y$ represents the cross section area parallel to the ground.

Furthermore, in order to obtain a rough rigid bed underneath the mobile sand cover, we deposit the mobile particles on top of a sheet of "frozen" immobile particles as displayed in Fig. 1 (see Suppl. Mat. for the set of DEM particle-particle contact force equations, including the presence of the frozen particles). In doing so, the rigid bed provides a model for a fully consolidated dune surface or bare granular surface, where the constituent immobile particles have the same diameter as the mobile grain size.

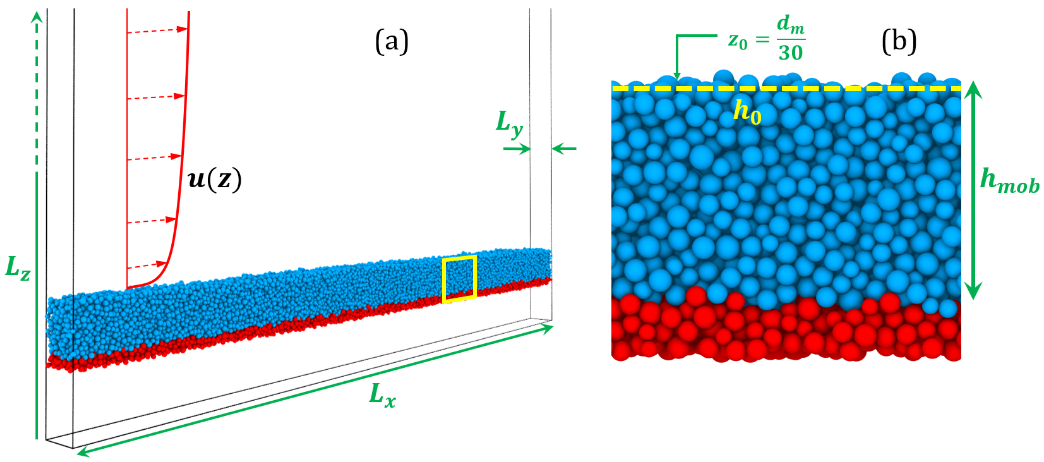

Figure 1: (a) Snapshot of the numerical experiment at $t = 0$, indicating the dimensions of the simulation domain and the undisturbed wind profile. (b) Side-view of an excerpt of the sediment bed, displaying a layer of mobile particles (blue) of thickness h_mob on top of the immobile particles constituting the rough ground.

3 Results and discussion

We find that the fully erodible bed scenario can be modeled by setting $h_{\mathrm{mob}} \gtrsim 15\,d_{\mathrm{m}}$. In particular, our simulations reproduce quantitively the value of the height-integrated, non-suspended mass flux of transported particles, Q, as a function of u_*, and the observation that, for moderate wind conditions ($u_*/u_{*\mathrm{t}} \lesssim 4$), Q is approximately proportional to $\tau - \tau_{\mathrm{t}}$, with $\tau = \rho_{\mathrm{f}} u_*^2$ denoting the mean shear stress of the turbulent wind flow over the surface, and $\tau_{\mathrm{t}} = \rho_{\mathrm{f}} u_{*\mathrm{t}}^2$ corresponding to the minimal threshold value of τ for sand transport (Fig. 2). Furthermore, our numerical predictions match the experimental observations of the nearly exponential decay of the vertical particle concentration profile above the ground and the minimal threshold wind shear velocity $u_{*\mathrm{t}} \approx 0.165\,\mathrm{m/s}$ predicted for the mean particle size in our simulations (see Suppl. Mat., Fig. S1).

However, we find that the scaling of Q with u_* changes as h_{mob} becomes smaller than about $15\,d_{\mathrm{m}}$. Indeed, wind tunnel experiments (Ho et al., 2011) revealed a cubic and a quadratic scaling of Q with u_* on rigid and on fully erodible beds, respectively. Here, we find that this scaling depends fundamentally on the thickness of the mobile sand layer on the ground, h_{mob}. Specifically, as shown in Fig. 2, we obtain the following scaling relation,

$$Q \propto (u_* - u_{*\mathrm{t}})^{p_Q} \cdot [\tau - \tau_{\mathrm{t}}], \tag{6}$$

where the exponent p_Q can be approximately described via,

$$p_Q = \exp\left\{-1.25\,\sqrt{h_{\mathrm{mob}}}\right\}. \tag{7}$$

To shed light on the microscopic origin of this nontrival scaling behavior, we note that momentum conservation yields $Q = [\ell_{\mathrm{hop}}/(u_{0\downarrow} - u_{0\uparrow})] \cdot [\tau - \tau_{\mathrm{t}}]$ (Bagnold, 1941; Sørensen, 2004; Ho et al., 2011), where ℓ_{hop} denotes the mean hop length of the saltating particles, while $u_{0\downarrow}$ and $u_{0\uparrow}$ are their mean horizontal impact and lift-off velocities, respectively.

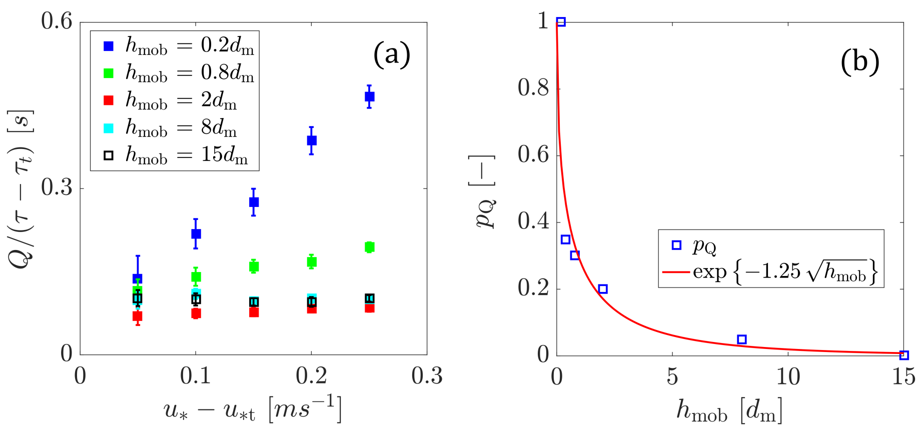

Figure 2: (a) Sand flux Q rescaled with the excess shear stress, $\tau - \tau_{\mathrm{t}}$, plotted as a function of $(u_* - u_{*\mathrm{t}})$ for different values of h_{mob}. (b) The symbols denote the exponent p_Q in Eq. (6) obtained from the best fit to the data in (a), while the continuous line denotes the exponential fit in Eq. (7).

Particles hitting the rigid bed rebound higher than upon impacting the fully erodible bed, because in the latter case, part of the impactor's momentum is transferred to mobilizing bed particles and producing a granular splash, thus leading to a lower coefficient of restitution

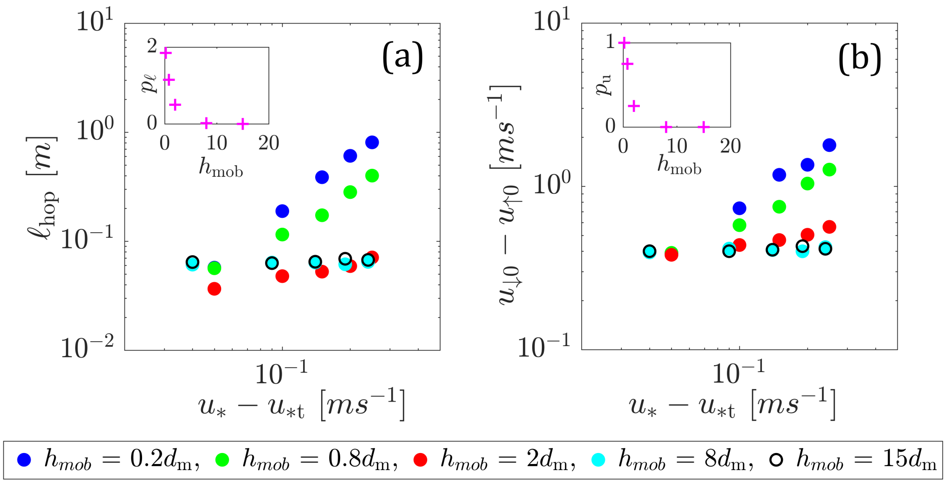

Figure 3: (a) Mean hop length ($\ell_{\rm hop}$) and (b) difference between the mean grain vertical velocities at impact and lift-off, $u_{0\downarrow} - u_{0\uparrow}$, as a function of $(u_* - u_{*\rm t})$. The insets indicate the respective exponents p_ℓ and $p_{\rm u}$ from the best fit using the expressions in Eq. (8).

(Rioual et al., 2000). Therefore, for a given saltation flux, the transport layer over the hard surface is much thicker, the particle concentration lower and the coupling between the air and the particles, thus, weaker than over the erodible bed (Ho et al., 2011). It was found in wind tunnel experiments that this weak coupling results in $\ell_{\rm hop}$ and $u_{0\downarrow} - u_{0\uparrow}$ over the rigid bed scaling with $(u_* - u_{*\rm t})^2$ and $(u_* - u_{*\rm t})$, respectively (Ho et al., 2011). By contrast, over a fully erodible bed, an increase in u_* leads to an enhancement of the particle concentration in the transport layer, without significantly affecting the mean grain velocity (Ho et al., 2011). However, our simulations reveal the following scaling laws for $\ell_{\rm hop}$ and $u_{0\downarrow} - u_{0\uparrow}$,

$$\ell_{\rm hop} \propto [u_* - u_{*\rm t}]^{p_\ell}\,, \qquad u_{0\downarrow} - u_{0\uparrow} \propto [u_* - u_{*\rm t}]^{p_u}\,, \tag{8}$$

with the exponents p_ℓ and p_u being a function of $h_{\rm mob}$ (Fig. 3),

$$p_\ell = 2\exp\{-0.67\,h_{\rm mob}\}\,, \qquad p_u = \exp\{-0.53\,h_{\rm mob}\}\,. \tag{9}$$

Therefore, as $h_{\rm mob} \to \infty$, i.e., in the dense sand bed scenario, p_ℓ, p_u and, thus, p_Q approach zero asymptotically and the scaling of Q with $\tau - \tau_{\rm t}$ is recovered (Fig. 2). Furthermore, as $h_{\rm mob} \to 0$, $p_\ell \to 2$ and $p_u \to 1$, so that $p_Q \to 1$, thus leading to the scaling of Q with $(u_* - u_{*\rm t}) \cdot [\tau - \tau_{\rm t}]$ observed for rigid beds (Ho et al., 2011). To the best of our knowledge, our study is the first one to address the scaling laws for the sediment transport rates for sand supply characterizing intermediate soil conditions between fully erodible and fully non-erodible. The knowledge of these scaling laws is essential for the parametrization of sediment transport and dust emission in climate models, in particular given the broad range of natural erodibility conditions associated with sparsely sand covered gravel, bare and crusted soils (Macpherson et al., 2008; Wang et al., 2011).

The scaling laws in Eq. (6) and (8) are consequence of the gradual expansion of the transport layer thickness as $h_{\rm mob}$ decreases below about $15\,d_{\rm m}$, which follows from the increase in the coefficient of restitution of particle-bed collisions as the bed becomes fully rigid (see Suppl. Mat., Fig. S3). Furthermore, we find that these scaling laws remain approximately valid when the rigid bed is a smooth flat surface, although the exponents are slightly different, $p_Q = A\exp\{-1.2\sqrt{h_{\rm mob}}\}$, $p_\ell = \exp\{-0.62\,h_{\rm mob}\}$ and $p_u = \exp\{-0.55\,h_{\rm mob}\}$.

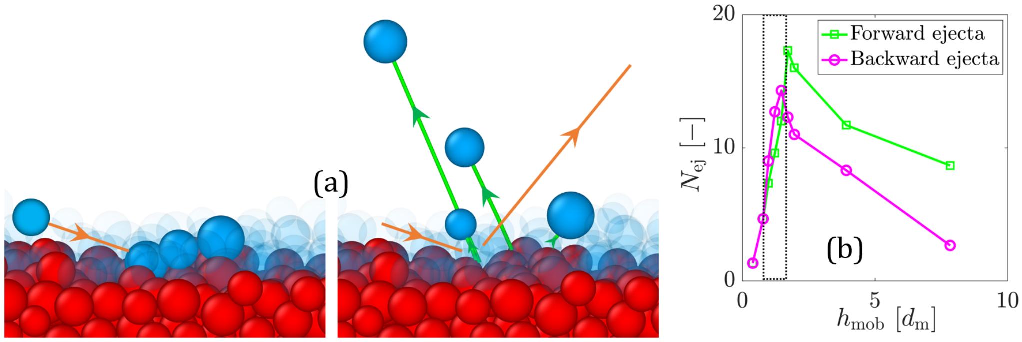

Figure 4: By means of granular splash numerical experiments with impact angles and velocities characteristic of wind-blown sand transport (a), we find that most ejected grains have negative horizontal lift-off velocity, when $h_{\mathrm{mob}} \lesssim 2\,d_{\mathrm{m}}$, and positive otherwise (b). The snapshots correspond to a simulation using $h_{\mathrm{mob}} \approx 2\,d_{\mathrm{m}}$. Most of the mobile (blue) particles lying on the rigid grains (red) have been rendered transparent for better visualization of the splashed particles.

However, the immobile roughness elements have a crucial effect on the value of the Aeolian sand flux, which we discuss next.

In the regime where $h_{\mathrm{mob}} \lesssim 2\,d_{\mathrm{m}}$, and in the presence of roughness elements on the ground, sand particles are ejected through splash events mainly *backwards*, i.e., the majority of ejecta displays negative horizontal lift-off velocity component. This result can be understood by noting that, as downwind hopping grains impact obliquely upon the thin sand layer covering the rough ground, they mobilize soil grains forward, which, however, collide with the roughness elements located in their front. Upon such collisions, the trajectories of the bed particles mobilized by grain-bed impacts are reflected backwards, as elucidated through our granular splash experiments (Fig. 4), thus yielding a negative mean horizontal lift-off velocity. These dynamics lead to an anomaly in the dependence of the sand flux Q on h_{mob}, with the emergence of a minimum flux value around $h_{\mathrm{mob}} \approx 2\,d_{\mathrm{m}}$, which is not observed when the ground is a smooth flat surface (Fig. 5). Furthermore the value of h_{mob} associated with the minimum flux is independent of u_*, thus indicating that the anomaly reported here is purely a signature of the soil erodibility conditions and is not affected by the flow properties.

Our model reproduces the different scaling laws of the Aeolian sand flux with the wind shear velocity observed experimentally, both over fully erodible and rigid beds (Figs. 2 and S1). However, various ingredients that are essential to improve the quantitative assessment of Aeolian sand flux, such as complex particle geometric shapes and aerodynamic entrainment (Li et al., 2020), should be incorporated in future work. Furthermore, we have employed sand-sized non-erodible roughness elements, but natural soils encompass much broader particle size distributions, including the presence of gravels, pebbles and rocks on the ground. Based on the results of our simulations, we expect that such coarser non-erodible elements have even larger impacts on the scaling laws of Aeolian sand transport rates. Our study is, thus, providing novel insights for future wind tunnel and numerical simulations to elucidate this impact, which is essential to reliably parametrizing wind-blown sand and dust on natural soils under supply limited conditions.

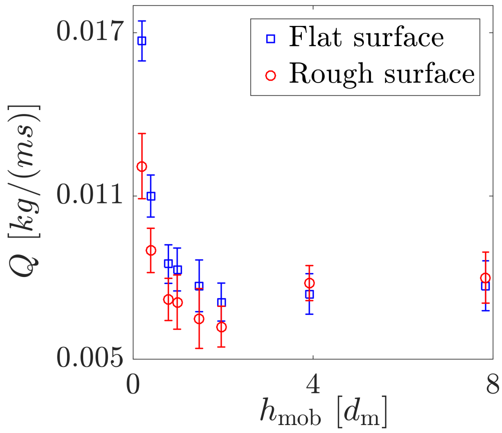

Figure 5: Sand flux Q as a function of h_{mob}, obtained with $u_* = 0.30\,\mathrm{m/s}$. We considered the non-erodible surface consisting of a smooth flat ground (blue) and immobile particles (red).

4 Conclusions

In conclusion, we have presented the first numerical model for wind-blown sand flux under supply limited conditions and found that this flux follows nontrivial, yet unreported scaling with the wind shear velocity, with scaling exponent determined by the mobile sand layer thickness. The roughness elements affect the scaling exponent of Q with u_* and cause an anomaly in the behavior of Q with h_{mob}, with the occurrence of a minimum which is independent on the flow conditions.

These findings will have an implication for the representation of non-erodible elements associated with different types of soil in future experimental and theoretical studies. Considering that the emission and transport of atmospheric dust aerosols constitute one of the main uncertainties in climate models, and that this dust is mainly ejected by Aeolian sand impacts onto the soil, the present work shall contribute a step toward more reliable dust schemes through a more accurate parametrization of Aeolian sand over natural soils. Furthermore, this study will hopefully inspire the elaboration of analytical models of Aeolian transport that accommodate the effect of coarser roughness elements, such as pebbles and rocks, on the scaling laws of Aeolian sand transport.

Acknowledgments

All data included in this work are generated from our numerical model and is available online (https://doi.org/10.6084/m9.figshare.14473848.v1). The data for validation with experiments is available from (Creyssels et al., 2009). We thank the German Research Foundation (DFG) for funding through the Heisenberg Programme and the grant - 348617785.

References

Almeida, M. P., Parteli, E. J. R., Andrade, J. S., & Herrmann, H. J. (2008). Giant saltation on mars. *Proceedings of the National Academy of Sciences*, *105*(17), 6222–6226. doi: https://doi.org/10.1073/pnas.0800202105

Amir, R., Kinast, S., Tsoar, H., Yizhaq, H., Zaady, E., & Ashkenazy, Y. (2014). The effect of wind and precipitation on vegetation and biogenic crust covers in the sde-hallamish sand dunes. *Journal of Geophysical Research: Earth Surface*, *119*(3), 437–450. doi:

https://doi.org/10.1002/2013JF002944

Anderson, R. S., & Haff, P. K. (1988). Simulation of eolian saltation. *Science*, *241* (4867), 820–823. doi: https://doi.org/10.1126/science.241.4867.820

Bagnold, R. A. (1941). *The physics of blown sand and desert dunes.* Methuen, London.

Carneiro, M. V., Pähtz, T., & Herrmann, H. J. (2011). Jump at the onset of saltation. *Physical Review Letters*, *107* (9), 098001. doi: https://doi.org/10.1103/PhysRevLett.107.098001

Cheng, N.-S. (2009). Comparison of formulas for drag coefficient and settling velocity of spherical particles. *Powder Technology*, *189* (3), 395–398. doi: https://doi.org/10.1016/j.powtec.2008.07.006

Comola, F., Gaume, J., Kok, J., & Lehning, M. (2019). Cohesion-induced enhancement of aeolian saltation. *Geophysical Research Letters*, *46* (10), 5566–5574. doi: https://doi.org/10.1029/2019GL082195

Creyssels, M., Dupont, P., El Moctar, A. O., Valance, A., Cantat, I., Jenkins, J. T., ... Rasmussen, K. R. (2009). Saltating particles in a turbulent boundary layer: experiment and theory. *J. Fluid Mechanics*, *625*, 47. doi: https://doi.org/10.1017/S0022112008005491

Cundall, P. A., & Strack, O. D. (1979). A discrete numerical model for granular assemblies. *geotechnique*, *29* (1), 47–65. doi: https://doi.org/10.1680/geot.1979.29.1.47

Durán, O., Andreotti, B., & Claudin, P. (2012). Numerical simulation of turbulent sediment transport, from bed load to saltation. *Physics of Fluids*, *24* (10), 103306. doi: https://doi.org/10.1063/1.4757662

Gillette, D. A. (1981). Production of dust that may be carried great distances. In *Desert Dust: Origin, Characteristics, and Effect on Man.* Geological Society of America. doi: https://doi.org/10.1130/SPE186-p11

Ho, T. D., Valance, A., Dupont, P., & El Moctar, A. O. (2011). Scaling laws in aeolian sand transport. *Physical Review Letters*, *106* (9), 094501. doi: https://doi.org/10.1103/PhysRevLett.106.094501

Kok, J. F., Parteli, E. J., Michaels, T. I., & Karam, D. B. (2012). The physics of wind-blown sand and dust. *Reports on progress in Physics*, *75* (10), 106901. doi: https://doi.org/10.1088/0034-4885/75/10/106901

Kok, J. F., & Renno, N. O. (2009). A comprehensive numerical model of steady state saltation (comsalt). *Journal of Geophysical Research: Atmospheres*, *114* (D17). doi: https://doi.org/10.1029/2009JD011702

Lämmel, M., Dzikowski, K., Kroy, K., Oger, L., & Valance, A. (2017). Grain-scale modeling and splash parametrization for aeolian sand transport. *Phys. Rev. E*, *95*, 022902. doi: https://doi.org/10.1103/PhysRevE.95.022902

Lämmel, M., Rings, D., & Kroy, K. (2012). A two-species continuum model for aeolian sand transport. *The New Journal of Physics*, *14* (9), 093037. doi: https://doi.org/10.1088/1367-2630/14/9/093037

Li, G., Zhang, J., Herrmann, H. J., Shao, Y., & Huang, N. (2020). Study of aerodynamic grain entrainment in aeolian transport. *Geophysical Research Letters*, *47* (11), e2019GL086574. doi: https://doi.org/10.1029/2019GL086574

Macpherson, T., Nickling, W. G., Gillies, J. A., & Etyemezian, V. (2008). Dust emissions from undisturbed and disturbed supply-limited desert surfaces. *Journal of Geophysical Research: Earth Surface*, *113* (F2). doi: https://doi.org/10.1029/2007JF000800

Mahowald, N., Albani, S., Kok, J. F., Engelstaeder, S., Scanza, R., Ward, D. S., & Flanner, M. G. (2014). The size distribution of desert dust aerosols and its impact on the earth system. *Aeolian Research*, *15*, 53-71. doi: https://doi.org/10.1016/j.aeolia.2013.09.002

Owen, P. R. (1964). Saltation of uniform grains in air. *Journal of Fluid Mechanics*, *20* (2), 225-242. doi: https://doi.org/10.1017/S0022112064001173

Pähtz, T., Parteli, E. J. R., Kok, J. F., & Herrmann, H. J. (2014). Analytical model for flux saturation in sediment transport. *Physical Review E*, *89* (5), 052213. doi: https://doi.org/10.1103/PhysRevE.89.052213

Rioual, F., Valance, A., & Bideau, D. (2000). Experimental study of the collision process of a grain on a two-dimensional granular bed. *Phys. Rev. E*, *62*, 2450–2459. doi: https://doi.org/10.1103/PhysRevE.62.2450

Sauermann, G., Kroy, K., & Herrmann, H. J. (2001). Continuum saltation model for sand dunes. *Physical Review E*, *64*(3), 031305. doi: https://doi.org/10.1103/PhysRevE.64.031305

Schepanski, K. (2018). Transport of mineral dust and its impact on climate. *Geosciences*, *8*(5). doi: https://doi.org/10.3390/geosciences8050151

Shao, Y. (Ed.). (2008). *Physics and modelling of wind erosion*. Springer Netherlands. doi: https://doi.org/10.1007/978-1-4020-8895-7

Shao, Y., & Li, A. (1999). Numerical modelling of saltation in the atmospheric surface layer. *Boundary-Layer Meteorology*, *91*, 199-225. doi: https:/doi.org/10.1023/A:1001816013475

Shao, Y., Raupach, M., & Findlater, P. (1993). Effect of saltation bombardment on the entrainment of dust by wind. *Journal of Geophysical Research: Atmospheres*, *98*(D7), 12719–12726. doi: https://doi.org/10.1029/93JD00396

Sørensen, M. (2004). On the rate of aeolian sand transport. *Geomorphology*, *59*(1-4), 53–62. doi: https://doi.org/10.1016/j.geomorph.2003.09.005

Wang, X., Zhang, C., Wang, H., Qian, G., Luo, W., Lu, J., & Wang, L. (2011). The significance of gobi desert surfaces for dust emissions in china: an experimental study. *Environmental Earth Sciences*, *64*(4), 1039–1050. doi: https://doi.org/10.1007/s12665-011-0922-2

Yin, X., Huang, N., Jiang, C., Parteli, E. J., & Zhang, J. (2021). Splash function for the collision of sand-sized particles onto an inclined granular bed, based on discrete-element-simulations. *Powder Technology*, *378*, 348-358. doi: https://doi.org/10.1016/j.powtec.2020.10.008

References from the Supporting Information

Brilliantov, N. V., Spahn, F., Hertzsch, J.-M., & Pöschel, T. (1996). Model for collisions in granular gases. *Physical review E*, *53*(5), 5382. doi: https://doi.org/10.1103/PhysRevE.53.5382

Carneiro, M. V., Araújo, N. A. M., Pähtz, T., & Herrmann, H. J. (2013). Midair collisions enhance saltation. *Physical review letters*, *111*(5), 058001. doi: https://doi.org/10.1103/PhysRevLett.111.058001

Di Renzo, A., & Di Maio, F. P. (2004). Comparison of contact-force models for the simulation of collisions in dem-based granular flow codes. *Chemical Engineering Science*, *59*(3), 525-541. doi: https://doi.org/10.1016/j.ces.2003.09.037

Fan, F., Parteli, E. J. R., & Pöschel, T. (2017). Origin of granular capillarity revealed by particle-based simulations. *Phys. Rev. Lett.*, *118*, 218001. doi: https://doi.org/10.1103/PhysRevLett.118.218001

Kruggel-Emden, H., Simsek, E., Rickelt, S., Wirtz, S., & Scherer, V. (2007). Review and extension of normal force models for the discrete element method. *Powder Technol.*, *171*, 157-173. doi: https://doi.org/10.1016/j.powtec.2006.10.004

Luding, S. (2008). Cohesive, frictional powders: contact models for tension. *Granular matter*, *10*(4), 235. doi: https://doi.org/10.1007/s10035-008-0099-x

Machado, M., Moreira, P., Flores, P., & Lankarani, H. M. (2012). Compliant contact force models in multibody dynamics: Evolution of the hertz contact theory. *Mechanism and Machine Theory*, *53*, 99-121. doi: https://doi.org/10.1016/j.mechmachtheory.2012.02.010

Parteli, E. J. R., Schmidt, J., Blümel, C., Wirth, K.-E., Peukert, W., & Pöschel, T. (2014). Attractive particle interaction forces and packing density of fine glass powders. *Sci. Rep.*, *4*, 6227. doi: https://doi.org/10.1038/srep06227

Plimpton, S. (1995). Fast parallel algorithms for short-range molecular dynamics. *Journal of computational physics*, *117*(1), 1–19. (Website of the DEM solver LAMMPS: `https://`

`lammps.sandia.gov/`) doi: https://doi.org/10.1006/jcph.1995.1039
Pöschel, T., & Schwager, T. (2005). *Computational granular dynamics*. Springer Berlin Heidelberg. doi: https://doi.org/10.1007/3-540-27720-X
Santos, A. P., Bolintineanu, D. S., Grest, G. S., Lechman, J. B., Plimpton, S. J., Srivastava, I., & Silbert, L. E. (2020). Granular packings with sliding, rolling, and twisting friction. *Phys. Rev. E*, *102*, 032903. doi: https://doi.org/10.1103/PhysRevE.102.032903
Schäfer, J., Dippel, S., & Wolf, D. E. (1996). Force Schemes in Simulations of Granular Materials. *J. Phys. I France*, *6*, 5-20. doi: https://doi.org/10.1051/jp1:1996129
Schmidt, J., Parteli, E. J., Uhlmann, N., Wörlein, N., Wirth, K.-E., Pöschel, T., & Peukert, W. (2020). Packings of micron-sized spherical particles: Insights from bulk density determination, x-ray microtomography and discrete element simulations. *Advanced Powder Technology*, *31*(6), 2293-2304. doi: https://doi.org/10.1016/j.apt.2020.03.018
Shao, Y., & Lu, H. (2000). A simple expression for wind erosion threshold friction velocity. *Journal of Geophysical Research: Atmospheres*, *105*(D17), 22437-22443. doi: https://doi.org/10.1029/2000JD900304
Silbert, L. E., Ertaş, D., Grest, G. S., Halsey, T. C., Levine, D., & Plimpton, S. J. (2001). Granular flow down an inclined plane: Bagnold scaling and rheology. *Physical Review E*, *64*(5), 051302. doi: https://doi.org/10.1103/PhysRevE.64.051302
Verbücheln, F., Parteli, E. J. R., & Pöschel, T. (2015). Helical inner-wall texture prevents jamming in granular pipe flows. *Soft Matter*, *11*(21), 4295–4305. doi: https://doi.org/10.1039/c5sm00760g